Electronic Supplementary Information

for

Mononuclear Iron(III) Complex with Unusual Temperature Change of Color and Magneto-Structural Properties: Synthesis, Structure, Magnetization, Multi-frequency ESR and DFT Study

by

Nitish Kumar Garg,[a] Yogesh Goriya,[a] Seetharaman Manojveer,[a] Senada Muratović,[b] Damir Pajić,[c] Mario Cetina,[d] Irina Petreska,[e] Yulia Krupskaya,[f] Vladislav Kataev,[f] Magnus T. Johnson,*[a] Ola F. Wendt*[a] and Dijana Žilić*[b]

[a] *Lund University, Department of Chemistry, P.O. Box 124, S-221 00 Lund, Sweden.*
[b] *Ruđer Bošković Institute, Bijenička cesta 54, 10000 Zagreb, Croatia.*
[c] *University of Zagreb, Faculty of Science, Department of Physics, Bijenička cesta 32, 10000 Zagreb, Croatia.*
[d] *University of Zagreb, Faculty of Textile Technology, Department of Applied Chemistry, Prilaz baruna Filipovića 28a, 10000 Zagreb, Croatia.*
[e] *Ss. Cyril and Methodius University in Skopje, Faculty of Natural Sciences and Mathematics - Skopje, Institute of Physics, PO Box 162, 1000 Skopje, Macedonia.*
[f] *Leibniz IFW Dresden, Helmholtzstrasse 20, D-01069 Dresden, Germany.*

E-mail:
magnus.johnson@chem.lu.se
ola.wendt@chem.lu.se
dijana.zilic@irb.hr

Contents

S1 Experimental **4**

S1.1 Synthesis . . . 4
S1.2 UV-Vis spectroscopy . . . 4
S1.3 Single crystal X-ray diffraction . . . 4
S1.4 Powder X-ray diffraction . . . 4
S1.5 Magnetization measurements . . . 5
S1.6 ESR spectroscopy . . . 5

S2 Results and discussion **6**

S2.1 Elemental analysis . . . 6
S2.2 UV-Vis spectroscopy . . . 6
S2.3 Single crystal X-ray studies . . . 6
S2.4 Powder X-ray diffraction . . . 10
S2.5 ESR spectroscopy . . . 11
S2.6 DFT study . . . 14

List of Figures

S1 UV-Vis absorption spectra recorded at room temperature and low temperature (∼100–150 K). . . . 6
S2 Molecular structure of the complex at RT, with atom numbering scheme. Displacement ellipsoids for non-hydrogen atoms are drawn at the 40% probability level. . . 7
S3 Overlapping diagrams of the complex at RT (red) and LT (blue): a) asymmetric unit of cation, and b) cation. Structures are overlapped through Fe1/O1/C2 atoms. Only two major components of disordered fluorine atoms of the complex at RT are shown. . . . 7
S4 Crystal packing diagram along the *b* axis of the complex at RT (red) and LT (blue), showing shorter distance between oxygen and hydrogen atoms of neighbouring parallel assemblies in LT. Structures are overlapped through Fe1/O1/C2 atoms. Only two major components of disordered fluorine atoms of the complex at RT are shown 8
S5 X-ray powder patterns of grounded crystals for the iron(III) complex recorded at 294 K compared to the simulated X-ray powder patterns at 295 K. . . . 10
S6 Temperature dependence of X-band ESR spectra of the Fe(III) complex with indicated *g*-factors of the pronounced lines. . . . 12
S7 Temperature dependence of HF-ESR spectra of the Fe(III) complex at the indicated temperatures. . . . 13

S8 Energy diagram with visualized orbitals HOMO-1, HOMO, LUMO and LUMO+1 of the studied complex (upper panel). Other neighboring frontier molecular orbitals with energies tabulated in Table S5 show very similar distribution. For illustration, orbitals LUMO+2 at both temperatures are shown in the lower panel. Ligand character is evident also in higher LUMOs, while lower HOMOs manifest mixed ligand-metal character. Localization of empty orbitals at RT is clearly seen in all neighboring frontier molecular orbitals. Presented results are obtained at pbe/6-31g(d,p) level of theory. 16
S9 HOMO-LUMO gap and visualization of HOMO (lower panels) and LUMO (upper panels) orbitals of the cation at two different temperatures. Presented results are obtained at pbe/6-31g(d,p) level of theory. 17

List of Tables

S1 Hydrogen-bonding geometries for the complex at RT and LT 6
S2 X-ray crystallographic data for the complex at RT and LT 9
S3 The spin-Hamiltonian parameters defined by spin-Hamiltonian 3 used for the simulation of ESR spectra recorded at X-band (9.6 GHz) and HF-ESR (252 GHz) frequencies. For all simulations $g = 2.00$ and $D = +2$ GHz (+0.067 cm^{-1}) are used. 11
S4 Comparison of the optimized energies of $[FeL_6](BF_4)_3$, obtained from DFT calculations, assuming different spin multiplicities. Energies for doublet and quartet states, respectively, are given relative to the sextet ground state. The optimized energies for the different spin multiplicities were evaluated at different levels of theory within the DFT methodology. 14
S5 Energies of the neighboring frontier molecular orbitals, obtained from DFT calculations on the experimental structures at RT and LT at pbe/6-31g(d,p) level of theory. 14
S6 Molecular orbital character obtained from full Mulliken orbital population analysis at pbe/6-31g(d,p) level of theory. Decomposition of HOMO orbitals by atoms showed around 30% of metal character, most of which falls on d-orbitals. The percentage of participation of d-orbitals in HOMO, as well as LUMO, and the nearest neighbors, at both temperatures, is summarized in this table. 15

S1 Experimental

S1.1 Synthesis

In a 50 mL round-bottom flask, 0.41 mmol (140 mg) of $Fe(BF_4)_2 \cdot 6H_2O$ was added to 2.47 mmol (270 mg) 2-hydroxy-6-methylpyridine in 25 mL dichloromethane. The reaction mixture was stirred for 1 h at room temperature which resulted in a dark reaction mixture. The solvent volume was reduced to ca. 10 mL and 1 mL pentane was added. The flask was covered with a rubber septum and kept inside the freezer at -23°C for crystallization. After 2 days, some cube like red crystals suitable for X-ray analysis were obtained which were separated and used for further characterization. No further attempts for quantitative isolation were made.

S1.2 UV-Vis spectroscopy

Solid-state absorption spectra were measured using Thermo Evolution 350 with cell Praying Mantis Diffuse Reflection Accessory - Harrick Scientific. Low temperatures were obtained by overflowing the sample with liquid nitrogen.

S1.3 Single crystal X-ray diffraction

Data for the investigated complex at RT and LT were collected on an Oxford Diffraction Gemini diffractometer with an EOS CCD detector using graphite monochromatized MoKα radiation (λ = 0.71073 Å) at 295 K and 125 K, respectively. The *CrysAlisPro*[1] program was used for data collection and processing. The intensities were corrected for absorption using the multi-scan absorption correction method.[1]The structures were solved with a dual-space algorithm using *SHELXT*,[2] and refined by full-matrix least-squares calculations based on F^2 using *SHELXL*[3] program integrated in the *Olex*2[4] program package. Hydrogen atoms were included in calculated positions and refined using riding model or a rotating group, with SHELXL[3] defaults. The whole structure of complex at LT is slightly disordered (ADPs are elongated in the same direction), what resulted in 1 checkCIF B level Alert. Fluorine atoms of tetrafluoroborate anion at RT are severely disordered over six sites, and were refined with fixed occupancy ratio in a range from 0.17 to 0.75. Restraint on anisotropic thermal parameters was applied in the refinement of boron and fluorine atoms at RT and fluorine atom at LT, as well as geometric restraint in the refinement on B–F distances at RT. Structures at RT and LT contain a total potential solvent area volume of 699.1 and 703.5 Å^3, respectively, with a small amount of solvent molecule(s) used for recrystallization (pentane). As they could not be modelled satisfactorily, data were treated with the *SolventMask* routine in *Olex*2.[4] PLATON[5]and Mercury[6] programs were used for structure analysis and drawing preparation. Details of crystal data, data collection, and refinement parameters are given in Table S2. CCDC 2098447 and 2098448 contain the supplementary crystallographic data for this paper. These data can be obtained free of charge from The Cambridge Crystallographic Data Centre via www.ccdc.cam.ac.uk/structures.

S1.4 Powder X-ray diffraction

PXRD data was obtained using the Panalytical Aeris Research tabletop diffractometer, with CuK radiation (40 kV and 7.5 mA) in the Bragg Brentano geometry.

S1.5 Magnetization measurements

Magnetization measurements were performed using a VSM-SQUID magnetometer from Quantum Design. The powder sample (smashed polycrystalline sample) was cooled in the zero-field cooled (ZFC) mode from room temperature down to 1.8 K, then $M(H)$ was measured in the field range from 0 to 7 T and back from 7 to 0 T. Finally, a field of 0.1 T was applied and $M(T)$ was measured upon heating the sample up to 300 K.

S1.6 ESR spectroscopy

X-band ESR experiments were performed with Bruker spectrometers EMX and Elexsys 580 FT/CW. The spectra of powder samples were recorded from room temperature down to liquid helium temperature, with a magnetic field modulation amplitude of 0.5 mT. HF-ESR experiments were obtained using a home-made spectrometer based on a Millimeterwave Vector Network Analyzer that produces millimetre- and submillimetre microwaves and allows phase locked detection of a signal. The HF-ESR spectrometer is equipped with a magnetocryostat (Oxford Instruments Ltd) with magnetic fields from 0 to 16 T. Due to a strong magnetization, the sample was diluted with sodium tetrafluoroborate by a ratio $\sim$1:10. The spectra were recorded from 3 K up to 150 K, at several selected frequencies in the range 170–318 GHz.

S2 Results and discussion

S2.1 Elemental analysis

The crystals were subjected to a microanalysis: Anal. Calcd. for $C_{36}H_{42}B_3F_{12}FeN_6O_6$: C, 44.53; H, 4.36; N 8.65. Found C, 43.62, H, 4.30; N 8.43. If there is a 2% salt impurity (e.g. $Fe(BF_4)_n$) the anal. calcd. is C, 43.62; H, 4.27; N 8.47, which fits reasonably well. We can thus imply a 98% bulk purity of the material.

S2.2 UV-Vis spectroscopy

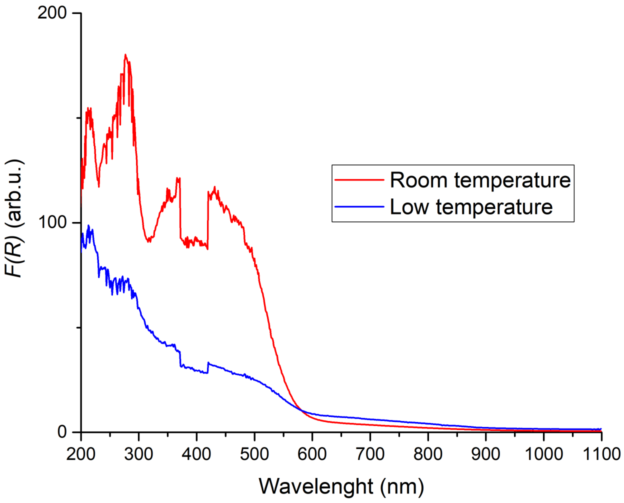

Fig. S1: UV-Vis absorption spectra recorded at room temperature and low temperature (∼100–150 K).

S2.3 Single crystal X-ray studies

Table S1: Hydrogen-bonding geometries for the complex at RT and LT

	D–H···A	D–H (Å)	H···A (Å)	D···A (Å)	D–H···A (°)	Symmetry code
RT[a]	C3–H3···O1	0.93	2.54	3.223(4)	131	-x+y, 1-x, z
	N1–H1···F1	0.86	1.97	2.826(7)	174	
LT	C3–H3···O1	0.95	2.51	3.209(9)	130	1-y, x-y, z
	N1–H1···F1	0.88	1.89	2.767(8)	173	
	C7–H7C···O1	0.98	2.63	3.559(12)	160	1-x, 1-y, 1-z
	C7–H7B···F2	0.98	2.44	3.374(15)	159	-2/3+y, -1/3+x, 7/6-z

[a] data for only two major components of disordered fluorine atoms are given

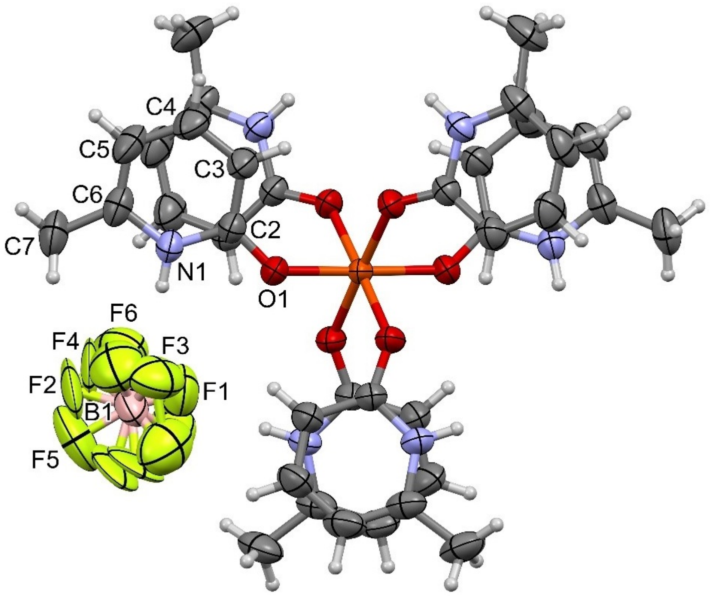

Fig. S2: Molecular structure of the complex at RT, with atom numbering scheme. Displacement ellipsoids for non-hydrogen atoms are drawn at the 40% probability level.

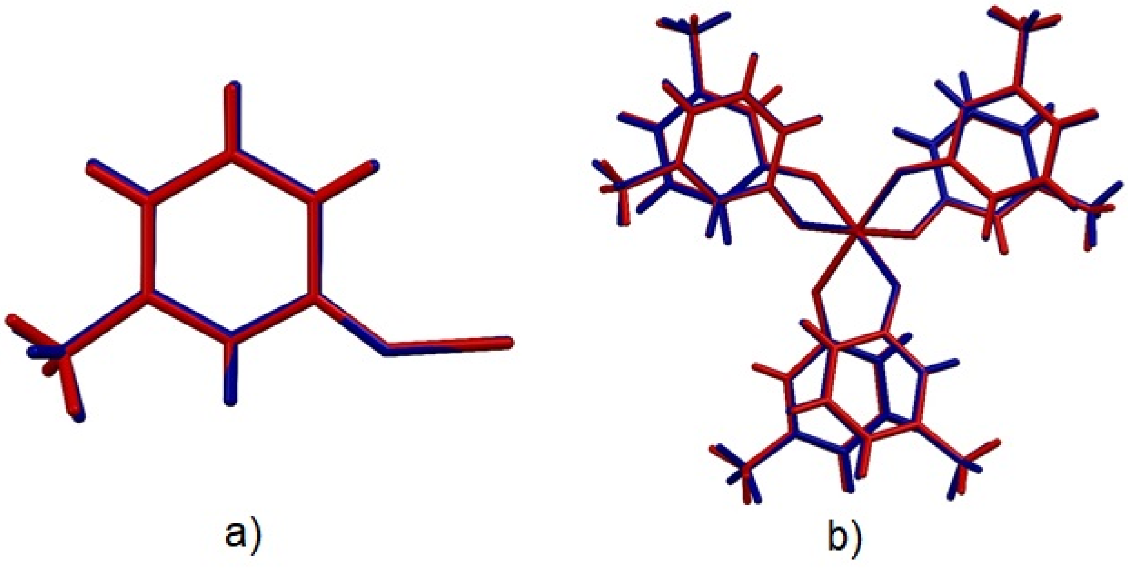

Fig. S3: Overlapping diagrams of the complex at RT (red) and LT (blue): a) asymmetric unit of cation, and b) cation. Structures are overlapped through Fe1/O1/C2 atoms. Only two major components of disordered fluorine atoms of the complex at RT are shown.

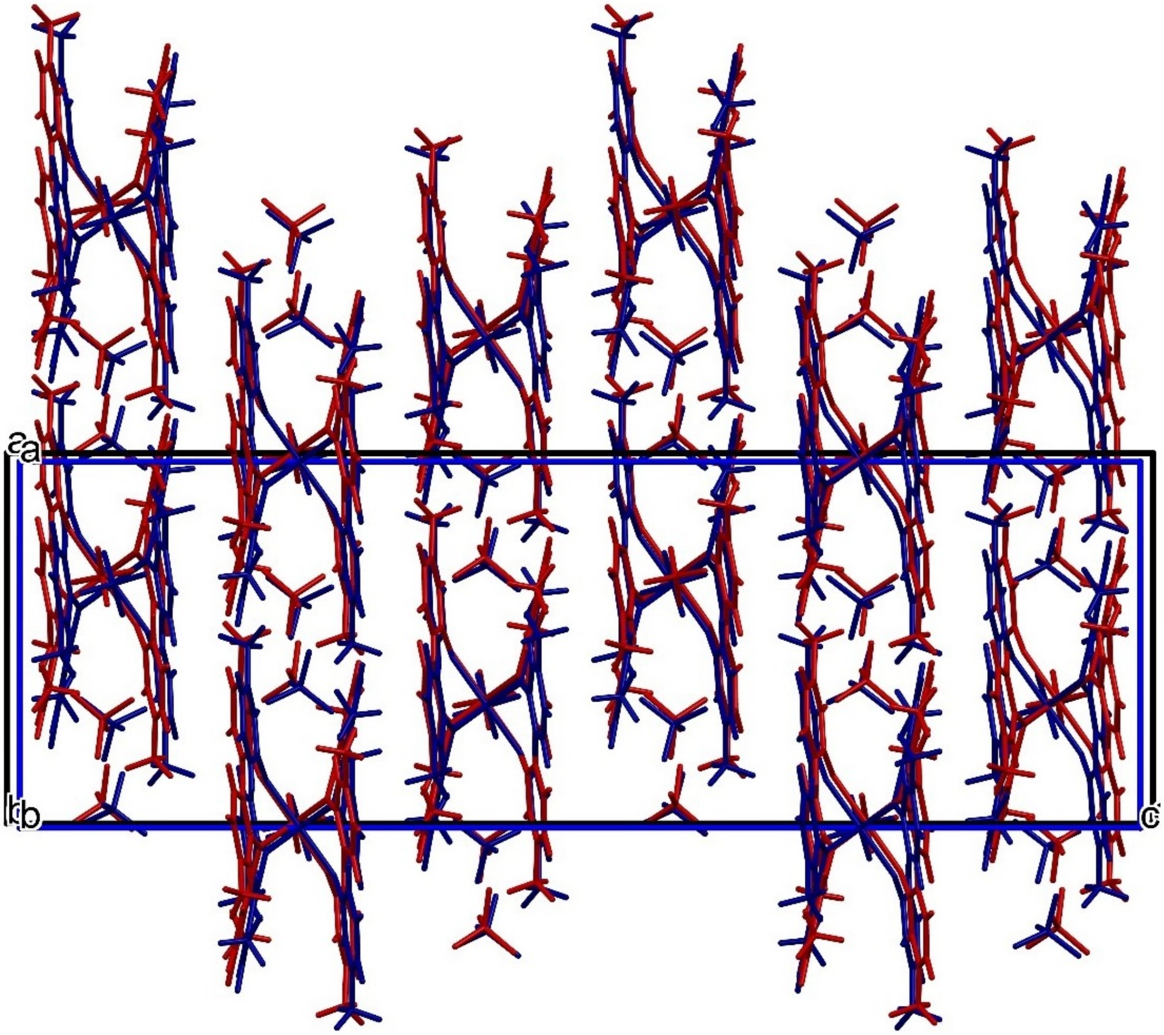

Fig. S4: Crystal packing diagram along the *b* axis of the complex at RT (red) and LT (blue), showing shorter distance between oxygen and hydrogen atoms of neighbouring parallel assemblies in LT. Structures are overlapped through Fe1/O1/C2 atoms. Only two major components of disordered fluorine atoms of the complex at RT are shown

.

Table S2: X-ray crystallographic data for the complex at RT and LT

	RT	LT
CCDC Number	2098447	2098448
Formula	$C_{36}H_{42}B_3F_{12}FeN_6O_6$	$C_{36}H_{42}B_3F_{12}FeN_6O_6$
Formula weight	971.03	971.03
T/K	295	125
Crystal system	trigonal	trigonal
Space group	R -3 c	R -3 c
Unit cell dimensions		
a/Å	14.5511(4)	14.3913(7)
b/Å	14.5511(4)	14.3913(7)
c/Å	39.000(2)	38.125(4)
$\alpha/^\circ$	90	90
$\beta/^\circ$	90	90
$\gamma/^\circ$	120	120
V/Å^3	7151.3(6)	6838.3(10)
Z	6	6
$D_{calc.}$/g cm^{-3}	1.353	1.415
Absorption coef.μ/ mm^{-1}	0.409	0.428
θ range for data collection/°	3.209-4.995	3.440-4.999
Collected reflections No.	24775	18022
Independent refl. No. / $R_{Int.}$	1412 / 0.0244	1341 / 0.0895
Reflections No. $I \geq 2\sigma(I)$	1165	744
Data^a/Restraints/Parameters	1412 / 36 / 131	1341 / 6 / 99
Goodness-of-fit on F^2, S	1.152	1.040
R [$I \geq 2\sigma(I)$]/R [all data]	0.0494 / 0.0580	0.0826 / 0.1360
wR [$I \geq 2\sigma(I)$] /wR [all data]	0.1503 / 0.1607	0.2167 / 0.2693
Max./min. el. density / e Å^{-3}	0.310 / -0.253	0.576 / -0.766

[a] Equal to independent reflections.

S2.4 Powder X-ray diffraction

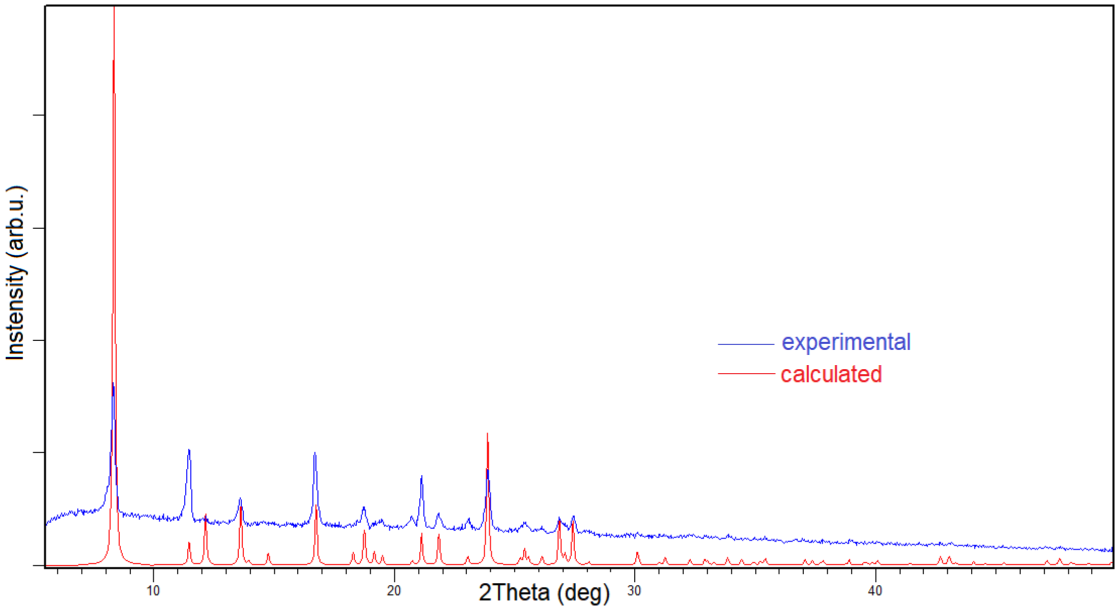

Fig. S5: X-ray powder patterns of grounded crystals for the iron(III) complex recorded at 294 K compared to the simulated X-ray powder patterns at 295 K.

S2.5 ESR spectroscopy

Table S3: The spin-Hamiltonian parameters defined by spin-Hamiltonian 3 used for the simulation of ESR spectra recorded at X-band (9.6 GHz) and HF-ESR (252 GHz) frequencies. For all simulations $g = 2.00$ and $D = +2$ GHz (+0.067 cm^{-1}) are used.

Frequency	T (K)	E/D	W_{pp} (mT)
X-band	300	0	20
X-band	220	1/13	20
X-band	150	1/4.7	30
X-band	78	1/4.5	30
X-band	5	1/4	20
HF-ESR	150	1/4.7	17
HF-ESR	100	1/4.5	18
HF-ESR	80	1/4.5	18
HF-ESR	50	1/4.5	18
HF-ESR	20	1/4.5	18
HF-ESR	3	1/4	10

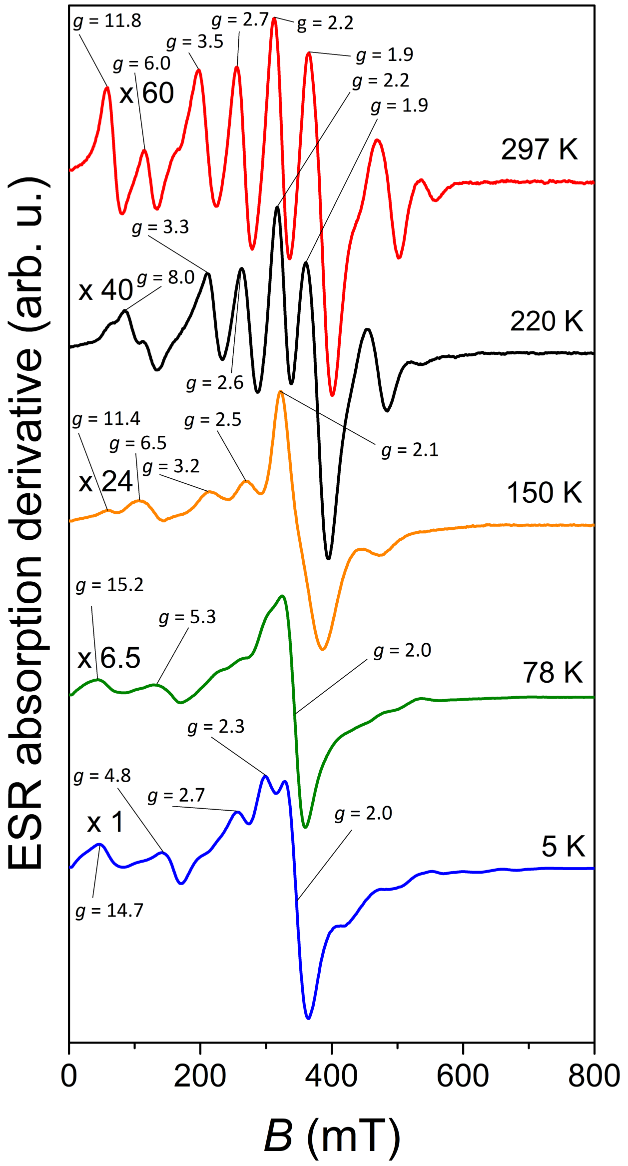

Fig. S6: Temperature dependence of X-band ESR spectra of the Fe(III) complex with indicated *g*-factors of the pronounced lines.

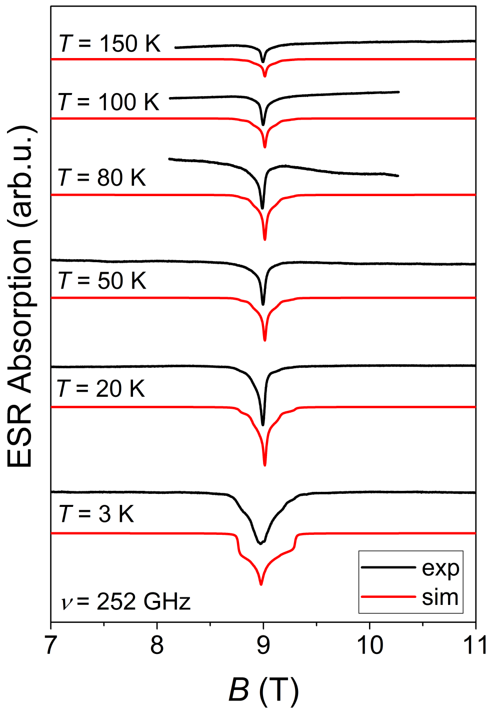

Fig. S7: Temperature dependence of HF-ESR spectra of the Fe(III) complex at the indicated temperatures.

S2.6 DFT study

Table S4: Comparison of the optimized energies of $[FeL_6](BF_4)_3$, obtained from DFT calculations, assuming different spin multiplicities. Energies for doublet and quartet states, respectively, are given relative to the sextet ground state. The optimized energies for the different spin multiplicities were evaluated at different levels of theory within the DFT methodology.

Method	2S+1	Energy (eV)	Energy (kcal/mol)
pbe/3-21g	2 4	1.67 1.34	38.51 30.90
pbe/6-31g(d,p)	2 4	1.10 0.89	25.37 20.52
B3LYP/6-31g(d,p)	2 4	1.42 1.14	32.75 26.29
B3LYP/6-311++g(2d,2p)	2 4	1.36 1.12	31.36 25.83

Table S5: Energies of the neighboring frontier molecular orbitals, obtained from DFT calculations on the experimental structures at RT and LT at pbe/6-31g(d,p) level of theory.

Molecular orbital	Energy (eV) 125 K	Energy (eV) 295 K	Energy (kcal/mol) 125 K	Energy (kcal/mol) 295 K
LUMO+4	-2.14	-2.12	-49.23	-48.87
LUMO+3	-2.15	-2.14	-49.63	-49.40
LUMO+2	-2.25	-2.31	-51.86	-53.29
LUMO+1	-2.27	-2.38	-52.32	-54.95
LUMO	-2.30	-2.48	-52.97	-57.17
HOMO	-5.25	-5.22	-121.09	-120.33
HOMO-1	-5.28	-5.27	-121.71	-121.41
HOMO-2	-5.67	-5.59	-130.71	-128.89
HOMO-3	-5.82	-5.61	-134.10	-129.42
HOMO-4	-5.84	-5.66	-134.67	-130.55

Table S6: Molecular orbital character obtained from full Mulliken orbital population analysis at pbe/6-31g(d,p) level of theory. Decomposition of HOMO orbitals by atoms showed around 30% of metal character, most of which falls on d-orbitals. The percentage of participation of d-orbitals in HOMO, as well as LUMO, and the nearest neighbors, at both temperatures, is summarized in this table.

T (K)	125	295	125	295	125	295	125	295
MO	HOMO-1	HOMO-1	HOMO	HOMO	LUMO	LUMO	LUMO+1	LUMO+1
d (%)	31	29	27	29	0.2	0.2	0.3	0.4

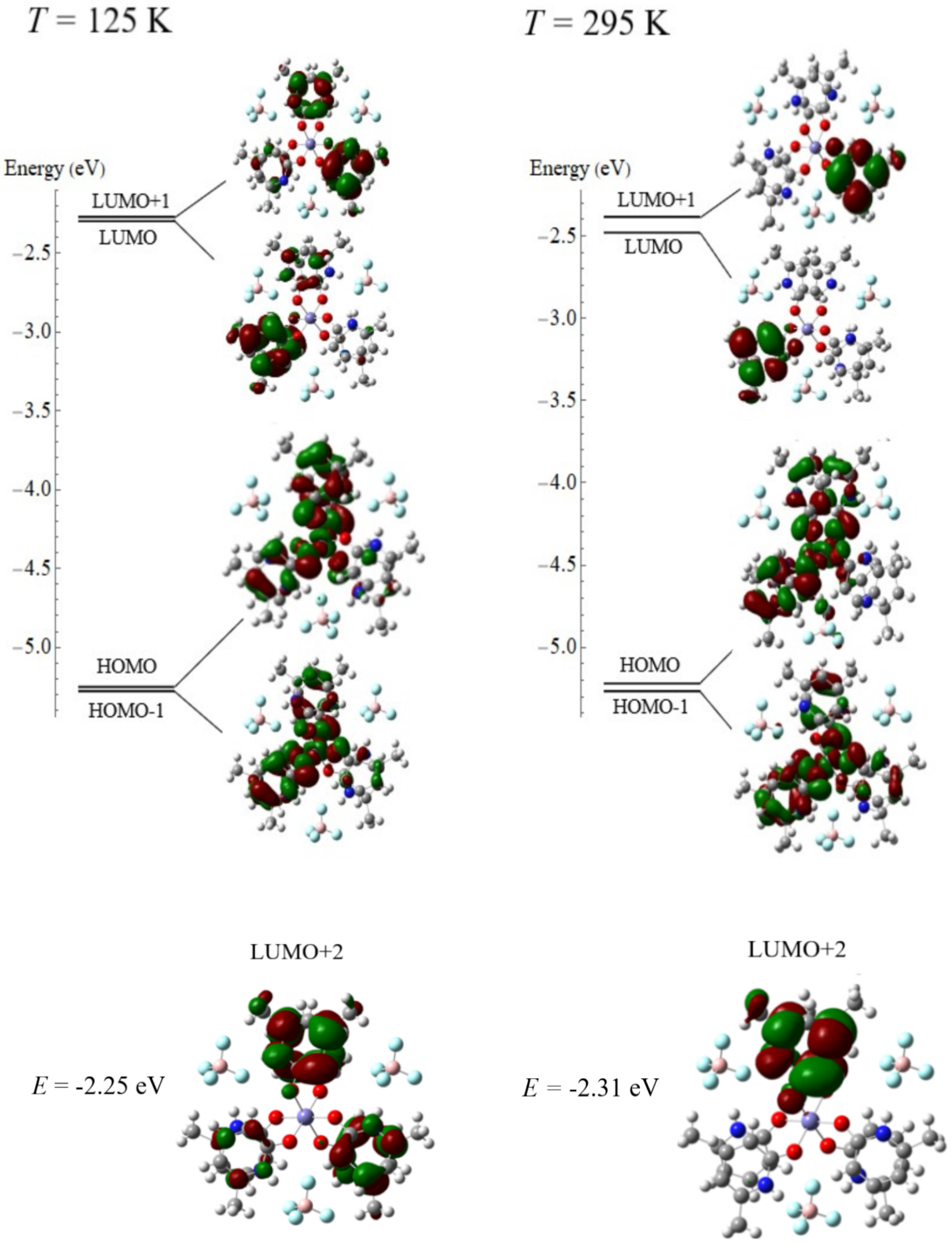

Fig. S8: Energy diagram with visualized orbitals HOMO-1, HOMO, LUMO and LUMO+1 of the studied complex (upper panel). Other neighboring frontier molecular orbitals with energies tabulated in Table S5 show very similar distribution. For illustration, orbitals LUMO+2 at both temperatures are shown in the lower panel. Ligand character is evident also in higher LUMOs, while lower HOMOs manifest mixed ligand-metal character. Localization of empty orbitals at RT is clearly seen in all neighboring frontier molecular orbitals. Presented results are obtained at pbe/6-31g(d,p) level of theory.

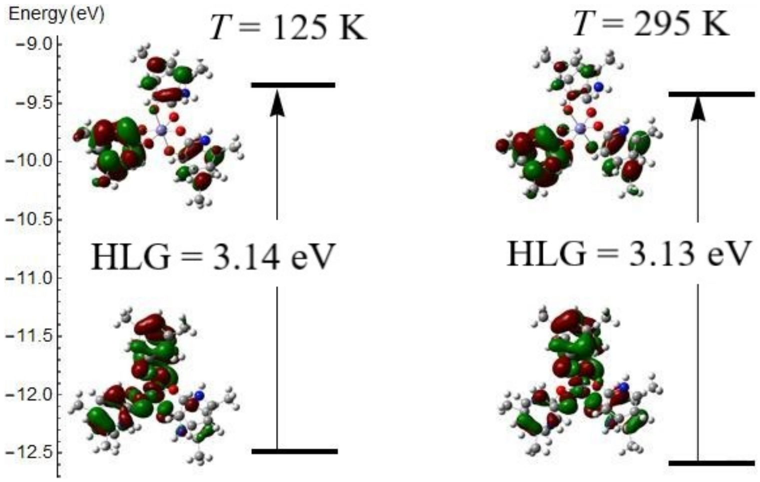

Fig. S9: HOMO-LUMO gap and visualization of HOMO (lower panels) and LUMO (upper panels) orbitals of the cation at two different temperatures. Presented results are obtained at pbe/6-31g(d,p) level of theory.

References

[1] *CrysAlis PRO*, Oxford Diffraction Ltd., U. K., 2007.

[2] G. M. Sheldrick, *Acta Cryst.*, 2015, **A71**, 3–8.

[3] G. M. Sheldrick, *Acta Cryst.*, 2015, **C71**, 3–8.

[4] O. V. Dolomanov, L. J. Bourhis, R. J. Gildea, J. A. K. Howard and H. Puschmann, *J. Appl. Cryst.*, 2009, **42**, 339–341.

[5] A. L. Spek, *Acta Crystallogr.*, 2009, **D65**, 148–155.

[6] C. F. Macrae, I. Sovago, S. J. Cottrell, P. T. A. Galek, P. McCabe, E. Pidcock, M. Platings, G. P. Shields, J. S. Stevens, M. Towler and P. A. Wood, *J. Appl. Crystallogr.*, 2020, **53**, 226–235.